Internal Proper-Motions in the Eskimo Nebula

Ma. T. García-Díaz[1], L. Gutiérrez[1], W. Steffen[1], J. A. López[1] and J. Beckman[2,3,4]

tere,leonel,wsteffen,jal@astro.unam.mx, jeb@iac.es

Received _____; accepted _____

To be submited to ApJ

[1]Instituto de Astronomía, Universidad Nacional Autónoma de México. Km 103 Carretera Tijuana-Ensenada, 22860 Ensenada, B.C., México

[2]Instituto de Astrofísica de Canarias. La Laguna, Tenerife, Spain.

[3]Consejo Superior de Investigaciones Científicas, Spain.

[4]Departamento de Astrofísica. Universidad de La Laguna. Tenerife, Spain

ABSTRACT

We present measurements of internal proper motions at more than five hundred positions of NGC 2392, the Eskimo Nebula, based on images acquired with WFPC2 on board the Hubble Space Telescope at two epochs separated by 7.695 years. Comparions of the two observations shows clearly the expansion of the nebula. We measured the amplitude and direction of the motion of local structures in the nebula by determining their relative shift during that interval. In order to assess the potential uncertainties in the determination of proper motions in this object, and in general, the measurements were performed using two different methods, used previously in the literature. We compare the results from the two methods, and to perform the scientific analysis of the results we choose one, the cross-correlation method, as the more reliable. We go on to perform a "criss-cross" mapping analysis on the proper motion vectors which helps in the interpretation of the velocity pattern. Combining our results on the proper motions with radial velocity measurements obtained from high resolution spectroscopic observations, and employing an existing 3D model, we estimate the distance to the nebula as 1299 pc.

Subject headings: Planetary Nebulae − NGC 2392 − Kinematic − techniques: spectroscopy − techniques: proper motion

1. Introduction

NGC 2392 (α = 07:29:10.76, δ = +20:54:42.47 [J2000.0]) is one of the most extensively studied high-ionization double-shell planetary nebulae (see García-Díaz et al. (2012), hereafter Paper I, and references therein) which is better known as the Eskimo nebula. The Eskimo nebula shows a very complex structure: a main inner shell with a filamentary shape surrounded by a ribbed structure (in Paper I "caps"), an outer shell, bright cometary knots and collimated high-velocity bipolar outflows.

Comprehensive spectroscopic kinematic studies in Paper I have shown that the expansion velocity of the inner shell is $V_{\rm exp}\approx \pm 120$ km s^{-1}. This kinematic study also revealed that the knots are distributed in a disk very near the plane of the sky expanding at velocities of $\approx$70 km s^{-1}. O'Dell et al. (1990) suggests that the outer shell is an oblate spheroid and the inner shell can be well described as a prolate spheroid oriented pole-on. In Paper I we found that the inner shell is tilted by 9° with respect to the line of sight with a position angle, P.A., of 25° and, to a first approximation, has a width to length ratio of approximately 1.8.

The central star (CS) of the Eskimo has been studied by several authors. An important discussion about the temperature of the CS is given by Pottasch et al. (2008), in a paper about the abundances of the nebula using spectral data obtained in the mid-infrared with the Spitzer Space Telescope. The authors assume that [N II] was formed probably in the first dredge-up, that the abundance of carbon was produced during the third dredge-up and that there is no evidence about the existence of a second dredge-up. From this analysis the authors found that the central star must have evolved from a progenitor of 1.7 $M_{\odot}$. Several authors have calculated an effective temperature, $T_{\rm eff}$, of the CS of around 40 000 K – 45 000 K (Méndez et al. 2011; Pauldrach et al. 2004; Kudritzki et al. 1997). However this temperature is not high enough to explain high stages of ionization of some

ions such as O IV and Ne V which have been observed in the nebula (Pottasch et al. 2008; Natta et al. 1980). Ciardullo et al. (1999) observed a weak companion of the CS which is undetected in V band. In an attempt to model the companion star, Danehkar et al. (2012) used photoionization models and their result showed that the companion star must have a T_{eff} = 250 000 K, which is much higher than that proposed by Pottasch et al. (2008). To date there is no decisive evidence on the nature of the putative companion star.

In order to understand the nature and origin of the Eskimo nebula, it is crucial to know its distance, which at present is not very well known. Several attempts have been made to find it using different statistical methods. Maciel (1981) estimated a distance of 1.1 kpc by using a mass-radius relation (Barker 1978). Hajian & Terzian (1995) measured the angular expansion of NGC 2392 at a radio frequency of 5 GHz with the VLA with 6 years between epochs, employing the Doppler expansion velocity to calculate the distance to the nebula (assuming a spherical shape). The authors did not detect an angular expansion of the nebula, leading to a lower limit for the distance of 1.4 kpc. Stanghellini et al. (2008) revised the calibration of the PN distance scale from Cahn et al. (1992) using data for PNe in the Magellanic Cloud. This statistical method is based on a calibration of the relation between the ionized mass (assuming that all nebulae have the same ionized mass) of PNe and the optical thickness parameter. In this way, the authors obtained a distance for NGC 2392 of 1.6 kpc with an uncertainty of 130 pc. Pottasch et al. (2011) reported 1.8 kpc for the distance, inferred from the core mass, the chemical nebular abundances, and the luminosity.

Another method for calculating distances is using proper motion measurements. Sample of a previous application of proper motion methods is found in Artigau et al (2011), who used cross-correlation methods to measure the proper motions of the knots and arcs of Eta Carinae using data from the Near-Infrared Coronagraphic Imager and NACO. Using the same method (cross-correlation), Ueta et al. (2006) calculated proper motions of the

dust shell structure in the Egg Nebula based on the archived two-epoch data at 2 μm taken with the Hubble Space Telescope (*HST*, with a 5.5 yr interval). From these data the authors determined the distance to the Egg nebula.

Szyszka et al (2011) used a different method on two epochs of *HST* imaging, separated by 9.43 yr in order to measure the expansion proper motions for NGC 6302's bipolar lobes, calculating the χ^2 of the difference image.

Li et al. (2002) observed the PN BD+30-3639 using the WFPC2 camera on board the *HST*. The data were obtained from two different epochs, separated by 5.663 yr. They used the χ^2 method to measure the radial expansion of this PN. To derive the distance of the nebula, these authors combined the angular expansion with radial expansion velocities taken from the *HST STIS* Echelle spectrograph.

A recent paper about proper motions was published by O'Dell et al. (2013), where tangential velocities were calculated for NGC 6720 using the least-squares (χ^2) method.

These studies all present the results of either only cross-correlation or the χ^2 method for their determination of internal proper motion patterns. Up to now it is, however, unclear how these methods compare and how consistent are the results when applied to the same data set. In order to asses better the reliability of proper motion measurements in general and for this object in particular by these methods, we apply both of them (cross-correlation and χ^2) on the same data sets.

In this paper, we report proper motion measurements for a large number of structures and arcs in the Eskimo nebula, using two [N II] 6584 Å images from the *HST* archive which were observed with a time interval of 7.695 yr. The results, along with the radial velocity measurements taken from long-slit, high-resolution, spectroscopic observations (Paper I) allow us to determine the distance.

The structure of the paper is as follows. In §2 we describe the observations and the data-reduction steps, including the alignment of the *HST* images. In §3 we describe in more detail the methods for finding the measurements of the proper motions in the nebula. In §3.1 we discuss the differences between the methods. In §4 we discuss the radial velocities. In §5 we explain the method for calculating the distance. In §6 we perform a criss-cross mapping analysis. Finally, we present in §7 and §8 a discussion of the results and our conclusions.

2. Observations and Data Reduction

2.1. High-resolution spectroscopy

For the present work, we used the data from Paper I. They are high-resolution spectroscopic observations of the Eskimo nebula obtained at the Observatorio Astronómico Nacional San Pedro Mártir (OAN-SPM), Baja California, México, during the nights of January 7–10, 2002. The data were obtained with the Manchester Echelle Spectrometer (Meaburn et al. 2003) attached to the 2.1 m telescope in its f/7.5 configuration. For all positions we used a 90 Å bandwidth filter to isolate the 87th order containing the Hα and [N II] nebular emission lines. For the majority of the exposures, we used a 70μm slit, while for some exposures a 150μm slit was applied. The slit was oriented north-south, and exposures were taken at a series of 18 different parallel pointings and three pointings at other position angles, P.A. = 70° (two positions) and P.A. = 110° (one position). The positions and orientations of the slit are shown in Figure 1 of Paper I. All spectra were acquired using exposure times of 1800 seconds. Full details of the observations and data reduction process are given in Paper I.

We convert heliocentric radial velocities to velocities relative to the Eskimo nebula by

taking the systemic velocity, $V_{\rm sys}$ = 70.5 km s^{-1}, calculated in Paper I. The spectroscopic data are summarized in Table 1.

Table 1: Log of spectroscopy observations from OAN-SPM

Position†	Data	Slit	PA
	yyyy/mm/dd	μm	$^{\rm o}$
a	2002-01-09	150	0
b – c	2002-01-08	70	0
d	2002-01-09	70	0
e	2002-01-08	70	0
f	2002-01-09	70	0
g	2002-01-07	70	0
h – n	2002-01-08	70	0
o – q	2002-01-09	70	0
r	2002-01-09	150	0
s	2002-01-10	70	110
t	2002-01-10	70	70
u	2002-01-10	70	70

†The Positions of the slit are shown in Figure 1 of Paper I

2.2. Hubble Space Telescope Data

The data used in this study to measure the proper motions of the Eskimo nebula consist of images which were retrieved from the *HST* archive. The observations were made in two separate observing runs: on January 1, 2000 (hereafter *Epoch-1*), as part of program 8499, with Andrew S. Fruchter as PI. During this run, three images were obtained with the

Wide Field Planetary Camara 2 (WFPC2), with exposure time 350 s, using (among others) the F658N filter. The second-epoch data were obtained on September 21, 2007 (hereafter *Epoch-2*), from the science program 11122, with Bruce Balick, as PI, who employed the same configuration as in program 8499 to acquire three images with the F658N filter, using 400 s exposure time for all of them. For all of the images we used the drizzled images (processed with Astrodrizzle). Table 2 summarizes the imaging observations.

Table 2: Log of photometry observations from *HST*

Date	Exposure	Dataset
yyyy/mm/dd	sec	
2000-01-11	350	u60v010er_drz
2000-01-11	350	u60v010fr_drz
2000-01-11	350	u60v010gr_drz
2007-09-21	400	ua010505m_drz
2007-09-21	400	ua010506m_drz
2007-09-21	400	ua010507m_drz

The time interval between observations is 7.695 yr with an angular resolution of $\approx 0\farcs1$. The mosaicing, geometric correction, and astrometry correction were done in the HST pipeline using Astrodrizzle. The mosaics were median combined. In order to compare the two combined mosaics, we regridded them using the SWARP utility (Bertin et al. 2002), matching the X-Y directions with RA-DEC. The correction of the very small residual relative displacements between the two mosaics were performed recursively by analyzing visually the arithmetic difference, using as reference the general structure that remains fixed. The shifting was carried out in 0.1-pix steps.

We used the central star as reference. The positions of the points where we calculated the proper motions in the nebula are given as offsets in RA and DEC referred to this point.

The resulting pictures are shown in Figure 1, which shows in the left and the center panels the two final images for each epoch (2000.03 and 2007.72 respectively) centered taking as reference the center of the Eskimo nebula, and the difference image from the two epochs in the right panel. In general, we can see that the arcs of the inner bubble have outwards motion from the star, whereas the knots of the outer shell have more modest movements than the arcs of the central bubble.

3. Measurement Technique

In order to measure the proper motions in the nebula, we determined the shift of > 500 regions, defined using well-defined knots or arcs. We used two methods based on the assumption that the proper motion of any local structure in a nebula due to expansion can be measured by determining the translational shift of the structure.

First method: This method employs cross-correlation, sometimes called *cross-covariance*. It is a measure of the similarity of two signals, in the one-dimensional case, or of two images, in the two-dimensional case. It is used mainly to look for patterns in an unknown signal comparing it with a known one.

The definition of the cross-correlation function $C_{fg}(i,j)$ normalized in a digital discrete image is given by:

$$C_{fg}(i,j) = \frac{\sum_{x=1}^{M}\sum_{y=1}^{N}\Big[f(x,y)-\bar{f}\Big]\Big[g(x-i,y-j)-\bar{g}\Big]}{\sigma_f \sigma_g} \qquad (1)$$

where $f(x,y)$ and $g(x,y)$ are functions representing the pixel values of the two images, i and j are the relative displacements of one image (*Epoch-2*) with respect to the other (*Epoch-1*), $\bar{f}$ and $\bar{g}$ are the average values of functions f and g, respectively, M and N are

the dimensions of the subimage used (in our case, instead of analyzing the entire image we analyzed sections of the image, and we refer to those as *subimages*), and σ_f and σ_g are their standard deviations. Then, $C_{fg}(i,j)$ varies between -1 and 1.

In this case, to calculate the velocity of a given point, we defined a *box* of size $N \times N$ pixels around that point, where N is chosen according to the characteristics of the neighborhood of the point. Generally, $N = 15$ was enough to measure the displacements of the points.

We denote as p the center of the box. This $N \times N$ pixels box is correlated with a box of the same size centered at $p + \delta$ in the other image. We then move δ so that $-\delta_{max} \leq \delta_x \leq \delta_{max}$ and $-\delta_{max} \leq \delta_y \leq \delta_{max}$, obtaining a value for the correlation at each point, to form the function $C(p, \delta)$. The point with coordinates (δ_x, δ_y) where the function is maximum determines the displacement of the structure under study.

Calculating the cross-correlation for different displacements, δ, in one of the images, we can build the function $C(p, \delta) = C_{fg}(\delta_x, \delta_y)$. For the calculations, we used the task XREGISTER implemented in IRAF, where the cross-correlation function is computed in the following manner:

$$C_{fg}(\delta_x, \delta_y) = \frac{\sum_{x=1}^{M} \sum_{y=1}^{N} \Big[f(x + \delta_x, y + \delta_y) - \bar{f} \Big] \Big[g(x, y) - \bar{g} \Big]}{\sigma_f \sigma_g} \tag{2}$$

where

$$\sigma_f = \Big[\sum_{x=1}^{M} \sum_{y=1}^{N} \Big[f(x + \delta_x, y + \delta_y) - \bar{f} \Big]^2 \Big]^{\frac{1}{2}} \tag{3}$$

$$\sigma_g = \Big[\sum_{x=1}^{M} \sum_{y=1}^{N} \Big[g(x,y) - \bar{g} \Big]^2 \Big]^{\frac{1}{2}} \tag{4}$$

$$\bar{f} = \frac{\sum_{x=1}^{M} \sum_{y=1}^{N} \Big[f(x+\delta_x, y+\delta_y) \Big]}{M \times N} \tag{5}$$

$$\bar{g} = \frac{\sum_{x=1}^{M} \sum_{y=1}^{N} \Big[g(x,y) \Big]}{M \times N} \tag{6}$$

Repeating the calculation in all the 536 regions marked on the *Epoch-1* image, we obtained the displacement map shown in Figure 2 (left panel), representing the internal motion of the nebula in the plane of the sky.

Second method: This method is based on the minimization of chi-squared (χ^2). We used the same 536 different local regions identified above.

These structures should be located at slightly shifted positions in the *Epoch-2* images due to proper motion of the nebula. To quantify the displacements, we defined square image sections centered on each of these local structures in the *Epoch-1* image. The size of these image sections has to be large enough so that the segmented structures can be uniquely identified. To analyze each section, we produced a custom IRAF task to shift the section of one epoch respect to the corresponding section of the other epoch, to calculate the difference and to estimate the chi squared (χ^2) on the difference. The script repeats this process spanning from $-\Delta x$ to $+\Delta x$, and from $-\Delta y$ to $+\Delta y$, where Δx and Δy were programable, in increments of 0.1 pixel. Visually we determined that the displacements are generally smaller than 1 pixel, so we carried out several trials putting $\Delta x = \Delta y = 2$ or 3 pixels. In Figure 3 we show a 3D plot of χ^2 for 12 example cases, where we can see that the surface shows a minimum value of χ^2 in these plots, which corresponds to the

displacement for which the region of the second epoch is most similar to the same region on the first epoch. Then measuring the position of this minimum gives the magnitud of the displacement vector, because the x,y coordinates of this point are the relative positions given in 0.1-pixel steps with respect to the center of the region on the *Epoch-1* image.

In general, the map obtained with this method (see Figure 2, right panel) is a good representation of the movements in the nebula. However, we found several cases where the minimum value is not so well defined as we can see in Figure 4. Generally in these cases the velocity vector was different from the movements observed in a visual approach. The reason for these discrepances could be the uncertainties in the determination of the displacements, given by the center of the surface of the χ^2 plot.

3.1. Differences between the two methods to calculate the proper motions.

We measured the proper motions of more than 500 regions of NGC 2392 by two methods: one using cross-correlation and another using the minimization of χ^2. There are several points where the magnitude of the displacement obtained by minimizing the χ^2 is larger than a full pixel, but visual inspection shows that the movements are smaller than that. We believe that these values, obtained by minimizing χ^2, are generally oversized in the process of searching the minimum value, particularly in regions where the shape of the surface defined by the value of χ^2 as a function of the displacements in X and Y is not as sharp and well behaved (see Figure 4) as those in Figure 3.

There are a couple of other points whose associated regions have very high ratio between the maximum and minimum values, or where this ratio is negative. In Figure 5 we show a plot of the ratio maximum/minimum of the pixel values in each subregion considered for each point in the χ^2 method, taken as a measure of the contrast. We see those cases in

Figure 5.

Discarding those points we see that in the overall, the discrepancy between these two methods is really small. However, we preferred the values obtained with the cross-correlation method since we did not need to discard any values with that method. In addition, comparing the two images using a direct visual approach, we can see that the values obtained from the cross-correlation method are more representative of the motion in the nebula, since the global proper motions are more readily apparent in the cross-correlation method.

4. Radial Velocities

The radial velocity of each local big structure or region (see Figure 1) was calculated using the [N II] 6584 Å line profile for 20 individual slit position originally used for Paper I. We identify each slit position over an *HST* [N II] image relating each component of the emission profile with the corresponding region of the *HST* image. In the position-velocity (P–V) arrays shown in Figure 2 of Paper I, we found several distinct regions distributed along the slit, Figure 6 shows an example of the distribution of the regions in slits i – l.

These regions include the jets but we did not use them because they are not visible in the *HST* images. We calculated the heliocentric velocity for each region by fitting a gaussian to the 1-D profile. The radial velocities are then calculated subtracting the systemic velocity. The errors in the determination of the velocities are given by the σ in each gaussian fitted, according to the relation $FWHM = 2\sqrt{2\ln(2)}\sigma$. The median of those values of σ is 10.5 km s^{-1}.

In some cases, we had problems with the identification of the velocities of some of the regions, because we found two or three different velocities in the same position of the *HST*

image. In those cases, we took the velocity of the brightest node in the P–V array.

The radial velocities with respect to the central star are listed in Table 3.

5. Distance

We calculate the distance to the Eskimo nebula using the proper motion vectors calculated from the cross-correlation method and taking only the vectors of the inner shell, given that we know its geometry. Statistically, the components of proper motions are $\langle pm_x \rangle \approx \langle pm_y \rangle$. If we consider a spherical distribution, the root mean square (RMS) of the radial velocity would be: $\langle rv \rangle \approx \langle pm_x \rangle \approx \langle pm_y \rangle$. Assuming the shape of the inner shell as modeled in Paper I (see Figure 7) where the ratio between the major axis (b) and minor axis (a) is b/a = 1.8, therefore,

$$\langle rv \rangle = (b/a)\,\langle pm_x \rangle = (b/a)\,\langle pm_y \rangle\,, \tag{7}$$

or, in terms of the RMS of the proper motions ($\langle pm \rangle = \sqrt{pm_x^2 + pm_y^2}$)

$$\langle rv \rangle = (b/a)\frac{\langle pm \rangle}{\sqrt{2}} \tag{8}$$

If we express the time interval between the two epochs of observation by δt (in years), the rms of the measured transverse displacements (on the images) by $\langle \delta r \rangle$ (in arcsec), and the distance D (in parsecs) to the Eskimo nebula, the rms of proper motions can be expressed by (see Appendix A, eq. 13),

$$\langle pm \rangle = 4.74\frac{D\ \langle \delta r \rangle}{\delta t} \tag{9}$$

Using the eq. 8, we can compute D by,

$$D = 0.211 \, \frac{\delta t}{\langle \delta r \rangle} \, \frac{\sqrt{2} \, \langle rv \rangle}{(b/a)} \tag{10}$$

and from our measurements we calculate a distance of 1299 pc. This value is similar to other published values: 1.4 kpc from Hajian & Terzian (1995), 1.6 kpc from Stanghellini et al. (2008) and 1.8 kpc from Pottasch et al. (2011).

Applying our newly computed distance, Table 3 lists the proper motion values converted from angular displacements to velocity in km s^{-1}, where we have used the scale factor to convert arcsec into km s^{-1} from Eq. 9 (801.3 km sec^{-1} $arcsec^{-1}$ calculated in Appendix A, Eq 17).

6. Criss-cross mapping

Criss-cross mapping was recently developed by Steffen & Koning (2011) as an analysis tool to identify patterns in proper motion measurements, in particular systematic deviations from homologous expansion. The basic idea is to find regions where the projected velocity vectors converge or diverge. For the mapping, the vectors are extended over the full image range independently of the direction. All lines have a fixed brightness value (e.g. 1) and are then added together in an image. The resulting image, which may be convolved with a gaussian smoothing function, will show enhanced values where the line crossing-points cluster, thereby revealing regions on which the motion converges or from where it diverges.

As can be appreciated by close inspection of Figure 2, the proper motion pattern obtained by applying the cross-correlation and the χ^2 methods are somewhat different from each other and clearly not consistent with the radial pattern expected from homologous expansion, which produces a central point-like concentration (Steffen & Koning, 2011). In

order to assess whether the deviations from homologous expansion are purely intrinsic to the methods or might contain information about deviations of the 3D velocity field from homologous expansion, we perform a criss-cross mapping analysis on the data and on a correction to the model of homologous expansion. The model is based on the following hypothesis.

Since the inner bubble of the Eskimo nebula contains hot X-ray emitting gas (Guerrero et al. 2005; Ruiz et al. 2013) it may well be that its expansion is dominated by thermal pressure. Therefore, instead of expanding homologously, the direction of the velocity field might be perpendicular at every surface point of the bubble. In Figure 7 (left panel) we therefore show the expected proper motion pattern for an axi-symmetric ellipsoid with axis ratio of 1.8 at an inclination angle of 20°, velocity vectors that are perpendicular to the local surface.

The predicted proper motion pattern is not unlike the observed pattern in that it contains strongly deviating vector directions and magnitudes very close to each other. This is because in this type of models the vectors from the front and back portions of the nebula may in fact have different magnitudes and directions at the same projected positions. In a homologous expansion the projections of all vectors onto the sky are radial, no matter what the orientation or whether they come from the front or back. For a more detailed qualitative analysis we apply the criss-cross mapping technique to the observations and this model (Figure 8).

The criss-cross map for the non-homologous ellipsoidal model shows a very characteristic pattern of an approximately straight line with uniform brightness along the direction of inclination (Figure 8, left). The criss-cross maps for the observations (Figure 8, middle and right) show a more complex structure centered to the north of the central star. The overall structure is, however, much less elongated in the north-south direction compared

to the ellipsoidal model and are more consistent with an off-center noisy point structure. The criss-cross mapping is therefore not consistent with an expansion perpendicular to the nebular surface but rather with radial expansion. The center of expansion is however off-center from the central star.

7. Discussion

In this article we have produced proper motion velocity maps for the Eskimo nebula, using images from the *HST* taken at two different epochs separated by 7.695 years. One map was generated using a method based on χ^2 minimization and the other was obtained by calculating the cross-correlation. Both methods used the same (> 500) subregions of the images. We find that the cross-correlation method provides a slightly more continuous pattern of proper motion vectors than the χ^2 method.

The X-ray emission, constrained by the outline of the inner bubble, suggests the possibility that the expansion of the bubble is dominated by the thermal pressure of the hot gas rather than by the inertia of the bubble, resulting in an expansion perpendicular to its surface, rather than radially outwards. A comparison with a simple ellipsoidal model with velocity vectors perpendicular to the surface shows that such a model indeed reproduces the overall local deviations of neighboring proper motion vectors.

Criss-cross mapping analysis is incompatible with the pressure driven overall ellipsoidal model and with the velocity perpendicular to the surface.

We also present the radial velocities calculated at the different points where we measured the proper motions. From those we infer a distance to the nebula of 1299 pc, a value well within the range of the published values (1.1 – 1.8 kpc) for the distance to this nebula.

8. Conclusions

A key result of this study is that the application of two different methods for the determination of internal proper motion in the Eskimo Nebula (NGC 2392) based on the same observational data has shown that the results are quite similar with minor deviations between the two methods.

Criss-cross mapping of the proper motion vector field yields no evidence in favor of an expansion perpendicular to the inner bubble, which in turn is an indication that the hot gas inside the bubble is not driving the expansion, rather than inertia of the dense shell of NGC 2392.

Last, but not least, based on our data we determined a distance to the Eskimo Nebula of approximately 1.29 kiloparsec.

Acknowledgments

This research has benefited from financial support from DGAPA-UNAM through grants IB100613-RR160613 and PAPIIT IN101014, as well as from Conacyt through grant 167236. We acknowledge the excellent support of the technical personnel at the OAN-SPM. This work is partially based on observations made with the NASA/ESA *Hubble Space Telescope*, obtained from the data archive at the Space Telescope Science Institute. STScI is operated by the Association of Universities for Research in Astronomy Inc., under NASA contract NAS5-26555. We thank the anonymous referee for the constructive comments that improved the presentation of this work.

Appendix A

Using our proper motion measurements, we are able to calculate the distance to the Eskimo nebula. Considering any distance subtended by an angle δr (in this case, δr is the measured transverse displacements in arcsec), as s. Then the distance, D to the Eskimo nebula is calculated by

$$\begin{aligned} s(\mathrm{km}) = D(\mathrm{km})\delta r(\mathrm{rad}) = 3.0856 \times 10^{13}(\mathrm{km\,pc^{-1}}) \\ \times D(\mathrm{pc})\,\frac{\delta r(\mathrm{arcsec})}{206264.8(\mathrm{arcsec/rad})}. \end{aligned} \tag{11}$$

Expressing the time interval between observations by δt, the RMS of the measured proper motions is given by

$$\begin{aligned} \left\langle pm(\mathrm{km\ s^{-1}})\right\rangle = \frac{S(\mathrm{km})}{\delta t(\mathrm{s})} = \\ \frac{3.0856 \times 10^{13}\, D(\mathrm{pc})\, \delta r(\mathrm{arcsec})\, /206264.8}{\delta t(\mathrm{yr}) \times 365.24 \times 24 \times 3600} \end{aligned} \tag{12}$$

$$\left\langle pm(\mathrm{km\ s^{-1}})\right\rangle = 4.7405\,\frac{D(\mathrm{pc})\,\delta r(\mathrm{arcsec})}{\delta t(\mathrm{yr})}. \tag{13}$$

Statistically, $\langle pm_x\rangle \approx \langle pm_y\rangle$, so with a spherical distribution $\langle rv\rangle \approx \langle pm_x\rangle \approx \langle pm_y\rangle$. However, assuming the shape of the inner shell as modeled in Paper I (where the major and minor axes are b and a), we can consider that, statistically, the RMS of the proper motions are b/a times the RMS of the radial velocities, $\langle rv\rangle$, i. e.

$$\langle rv\rangle = b/a\,\langle pm_x\rangle = b/a\,\langle pm_y\rangle\,, \tag{14}$$

or

$$\langle rv\rangle = b/a\frac{\langle pm\rangle}{\sqrt{2}}. \tag{15}$$

Then the distance to the nebula is

$$D(\mathrm{pc}) = 0.211\frac{\delta t(\mathrm{yr})}{\delta r(\mathrm{arcsec})}\frac{\sqrt{2}\left\langle rv(\mathrm{km\ s^{-1}})\right\rangle}{(b/a)}. \tag{16}$$

taking b/a = 1.84 which was derived from the 3D model (Paper I), we final $D = 1299$ pc. If we consider $\delta t = 8.805$ yr, we are able to calculate a scale factor to convert arcsec into km s^{-1} from Eq. 13

$$\left\langle pm(\text{km s}^{-1})\right\rangle = 801.3\,\delta r(\text{arcsec}) \tag{17}$$

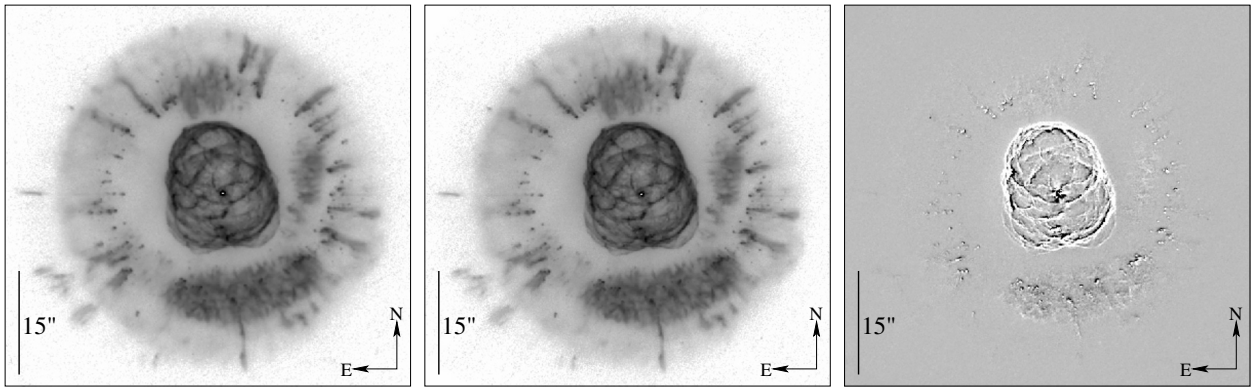

Fig. 1.— Left: *Epoch-1* image [N II] WFPC2-*HST*. Center: *Epoch-2* image [N II] WFPC2-*HST*. Right: Difference of the two images taken 7.695 yr apart (2007-2000). In the difference image, the central bubble with proper motions shows up as "negative/positive" double ridge structures.

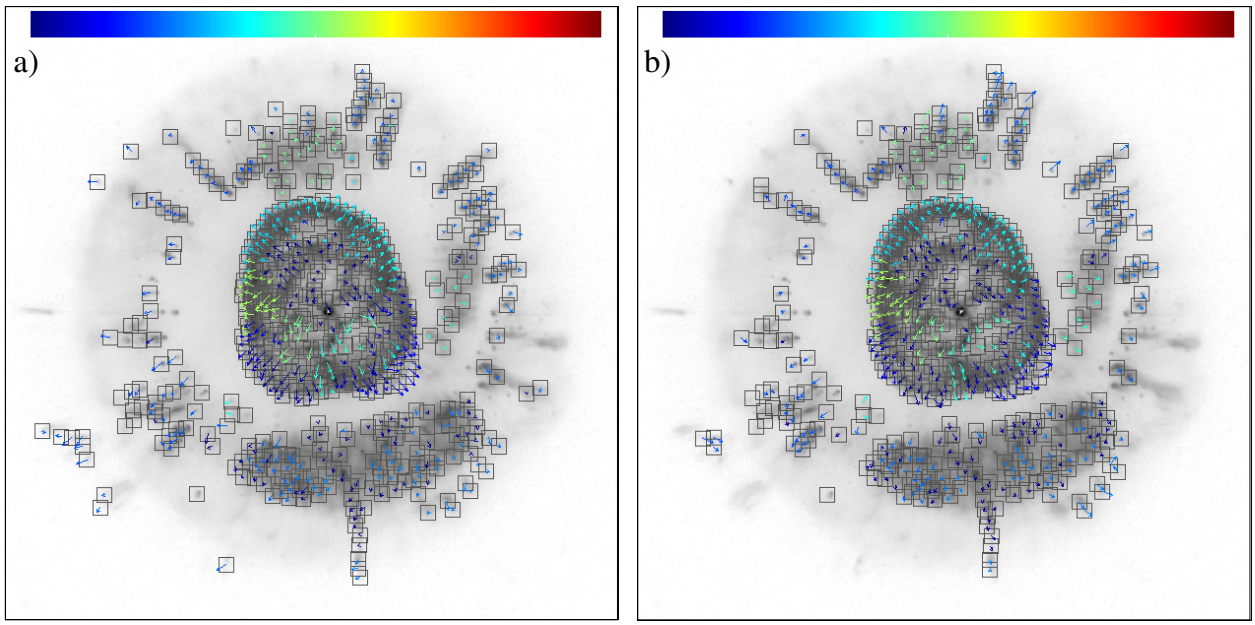

Fig. 2.— *Left panel:* Map of proper motions obtained with the cross-correlation method. *Right panel:* Map of proper motions obtained with the χ^2 method

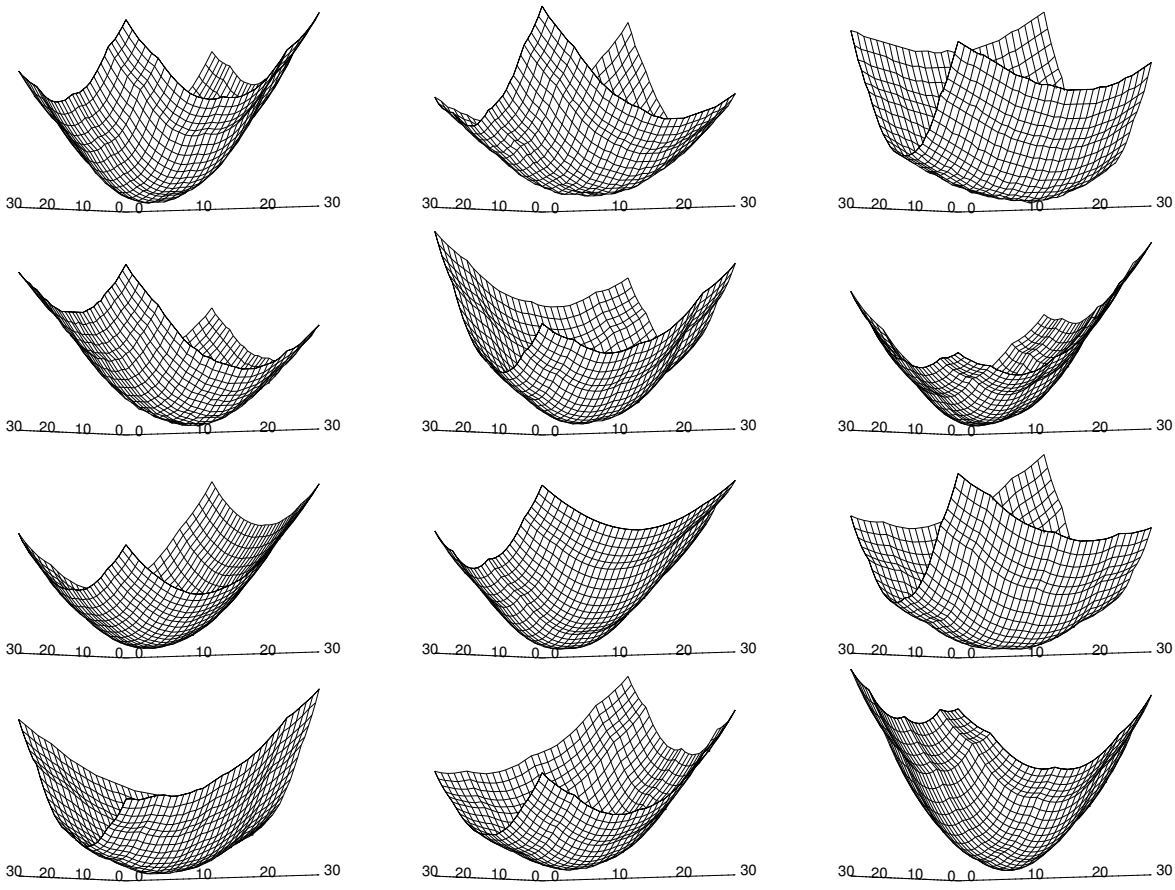

Fig. 3.— Some of the 3-D plots of chi-squared as a function of the displacements in X and Y. The scale of the Z axis is in arbitrary units. In this figures we can see the minimum very well defined.

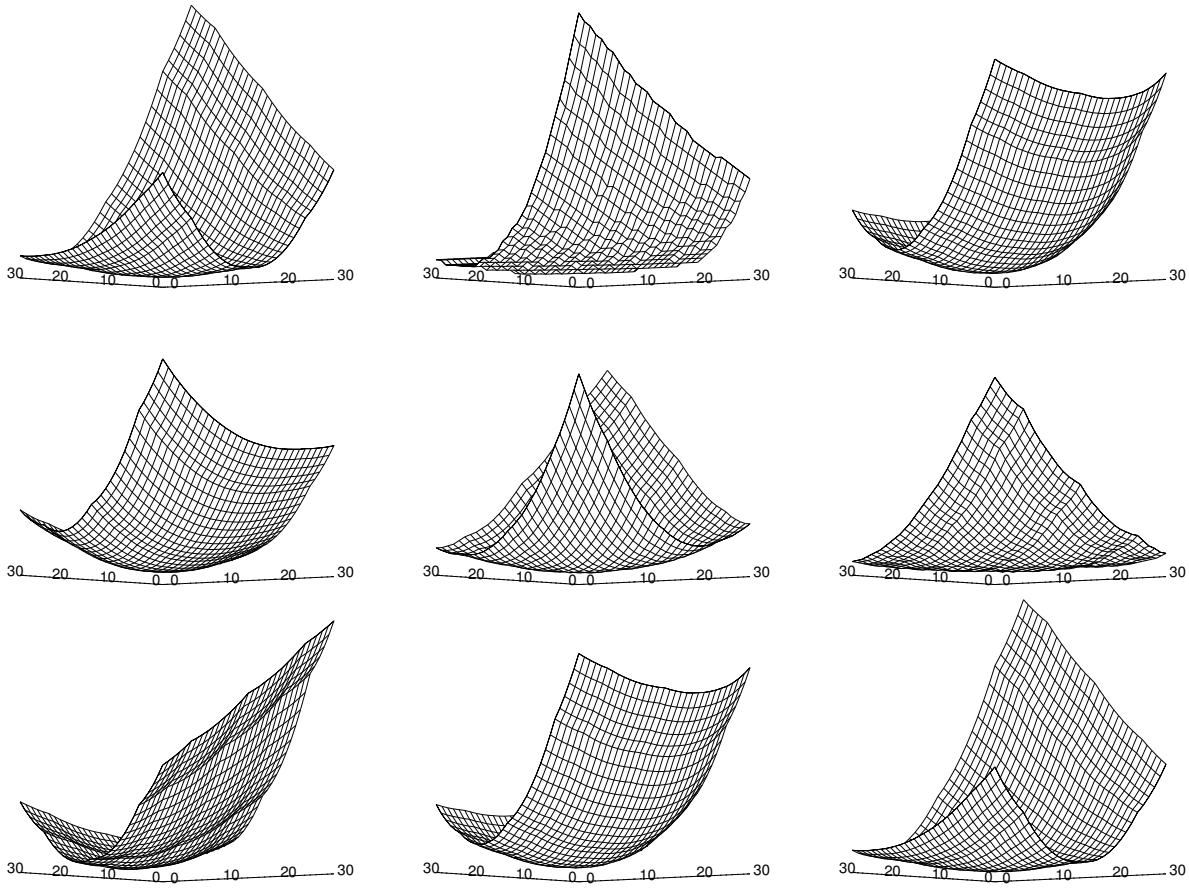

Fig. 4.— Same as Fig. 4, but can be noticed that in this case the function around the minimum is more difficult to be defined. In several of these cases the calculated velocity vector was different than the movement observed using a visual approach.

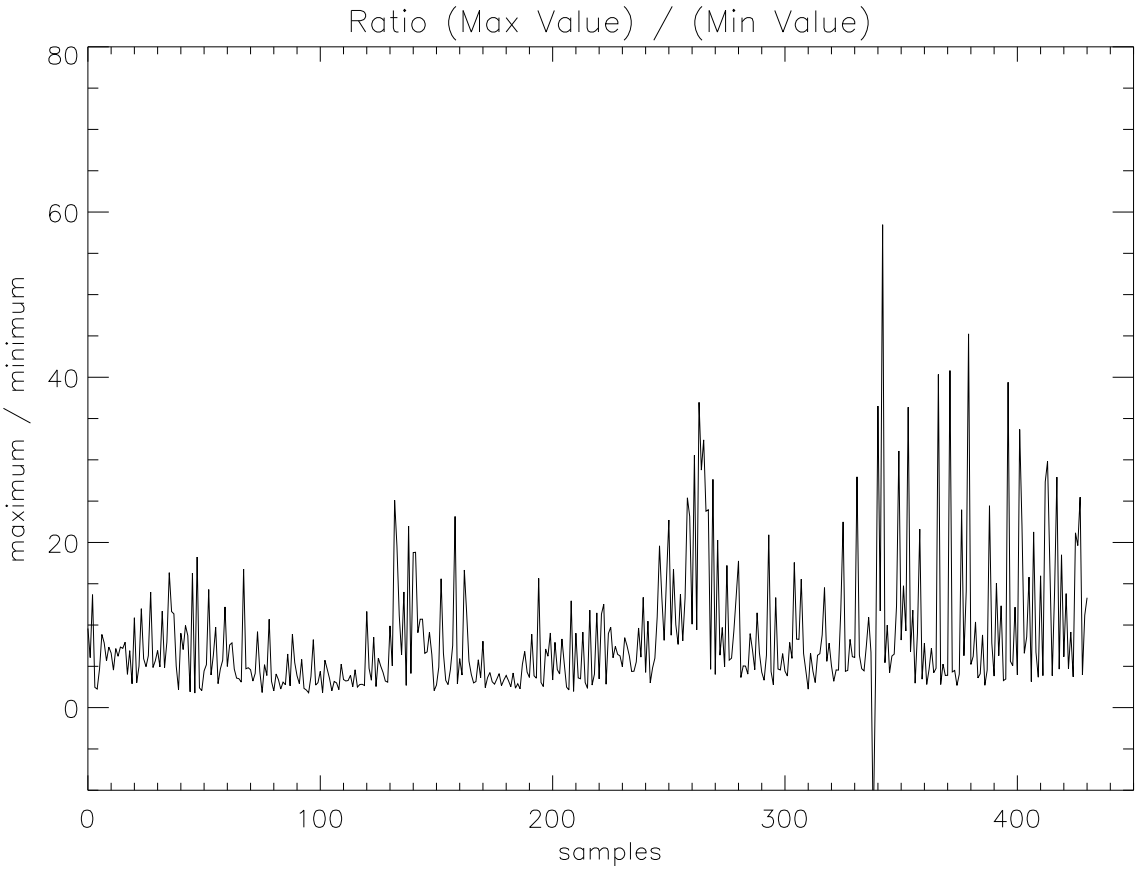

Fig. 5.— A plot of the ratio *maximum/minimum* value for the pixels for each of the 536 regions selected in the χ^2 method, having discarded those for which the magnitude of the displacement is larger than a full pixel. We can see that in some cases this ratio is very large or negative. The larger and the minimum values correspond in this case to regions near of the central star, where we found saturated pixels.

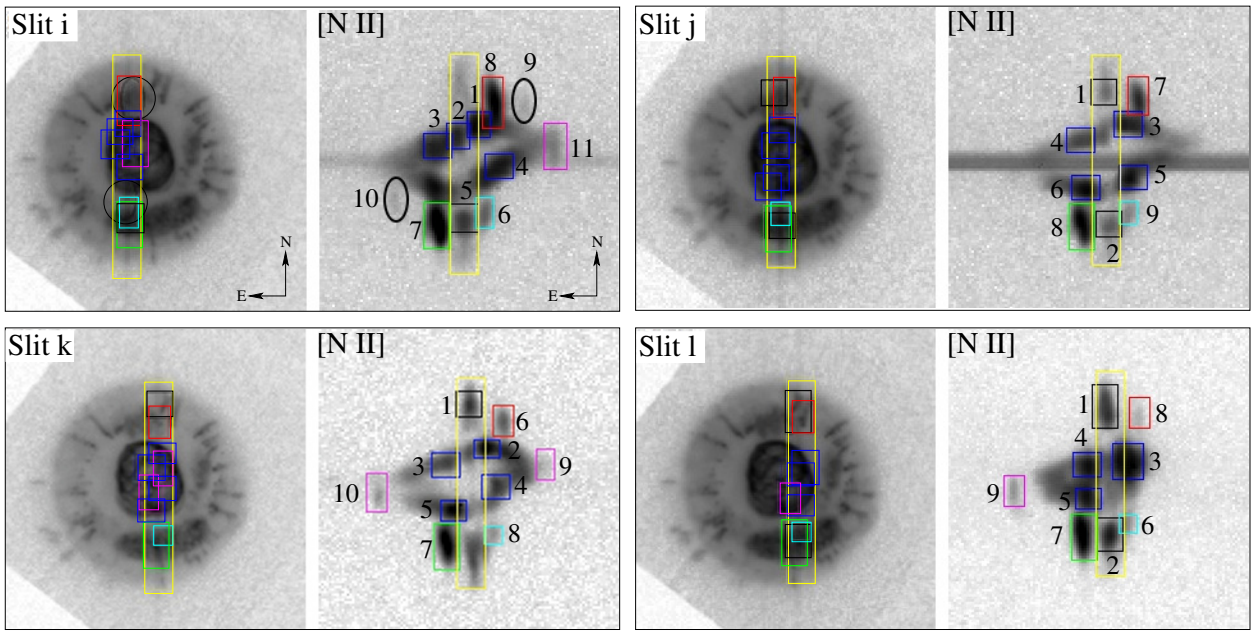

Fig. 6.— Example of regions on slits i l where we measured the radial velocity. Details about these observations are in Paper I.

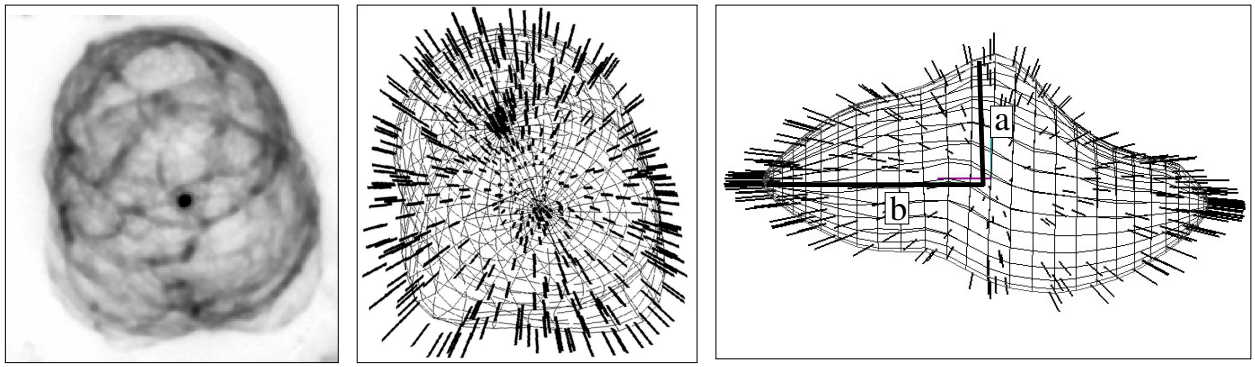

Fig. 7.— The inner bubble of Eskimo nebula and the velocity vectors according to the model (Paper I).

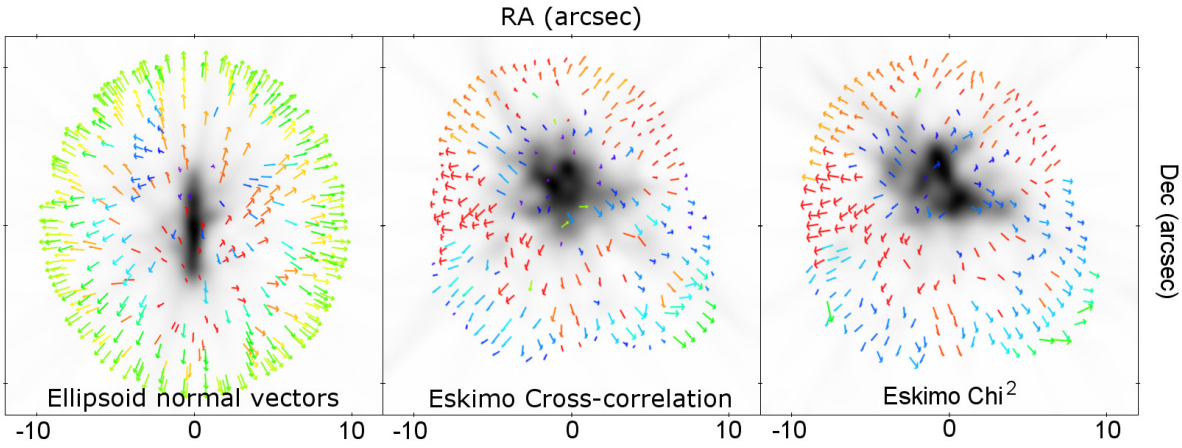

Fig. 8.— The criss-cross maps for the ellipsoidal model (left panel) and the measured values for the cross-correlation and χ^2 methods in the middle and on the right, respectively.

Table 3: Columns 1 and 2 give the position of each region, referred to the central star. Columns 3 and 4 give the proper motion in pixels of each knot. Columns 5 and 6 contain the proper motions in km s^{-1}. Column 7 gives de magnitud of the proper motion vector in km s^{-1}. Column 8 gives the radial velocity in km s^{-1} calculated from high resolution spectra (the full table is in the online version of this paper).

(1)	(2)	(3)	(4)	(5)	(6)	(7)	(8)
X	Y	pm_x	pm_y	pm_x	pm_y	Proper Motion	Radial Velocity
arcsec	arcsec	(pix)	(pix)	(km s^{-1})	(km s^{-1})	(km s^{-1})	(km s^{-1})
25.94	-12.02	0.4210	0.3641	33.76	29.20	47.74	-5.50
24.87	-12.82	0.3913	0.1027	31.38	8.24	44.38	-2.80
24.87	-11.92	0.2686	0.4216	21.54	33.81	30.46	-2.80
24.44	-14.12	0.4829	0.1922	38.72	15.41	54.76	-2.80
23.37	12.18	0.4522	-0.0030	36.26	-0.24	51.28	-5.10
23.05	-18.62	0.1641	0.2169	13.16	17.39	18.61	0.20
22.62	-17.42	0.1062	0.0486	8.52	3.90	12.04	0.20
22.08	-2.52	0.4363	-0.0529	34.99	-4.24	49.48	-5.50
20.91	-8.22	0.2596	0.0559	20.82	4.48	29.44	···
20.59	-10.92	0.2903	-0.1512	23.28	-12.12	32.92	···
20.59	-2.72	0.4351	0.2505	34.89	20.09	49.34	···
20.37	-16.82	-0.0935	0.1247	-7.50	10.00	10.60	···
20.16	-17.82	0.1391	0.1053	11.15	8.44	15.78	···
20.05	11.08	0.1588	-0.1636	12.73	-13.12	18.01	···
20.05	11.88	0.1974	-0.2830	15.83	-22.69	22.39	···
19.94	-1.42	0.3877	0.1159	31.09	9.29	43.97	···
19.94	15.08	0.2191	-0.2212	17.57	-17.74	24.85	-3.80
19.84	-7.62	0.1277	0.2136	10.24	17.13	14.48	-5.30
19.73	-9.42	0.0458	0.2229	3.67	17.87	5.19	···
19.62	-10.32	0.0679	0.0536	5.45	4.30	7.70	···

REFERENCES

Artigau, Étienne, Martin, John C., Humphreys, Roberta M., Davidson, Kris, Chesneau, Olivier,& Smith, Nathan. 2011, AJ, 141, 202A

Baldwin, J. A., Verner, E. M., Verner, D. A., Ferland, G. J., Martin, P. G., Korista, K. T., & Rubin, R. H. 2000, ApJS, 129, 229B

Barker, T. 1978, ApJ, 291, 914

Bertin E., Mellier Y., Radovich M., Missonnier G., Didelon P., Morin B., 2002, in Astronomical Data Analysis Software and Systems XI, ASP Conf. Series 281, 228.

Ciardullo, R., Bond, H. E., Sipior, M. S., Fullton, L. K., Zhang, C.-Y., Schaefer, K. G. 1999, AJ, 118, 488

Cahn, J. H., Kaler, J. B. and Stanghellini, L. 1992, AASS. 94, 399

Danehkar, A., Frew, D. J.; De Marco, O., & Parker, Q. A. 2011in "From Interacting Binaries to Exoplanets: Essential Modeling Tools", I eds. Richards, M. T. and Hubeny, 2012 IAU Symp. 282, 470

García-Díaz, M. T., López, J. A., Steffen, W., & Richer, M. G. 2012, ApJ, 761, 172G

Hajian, A. R., & Terzian, Y. 1995, AJ, 109, 2600

Heap, S. R. 1977, ApJ, 215, 864

Kudritzki, R. P., Mendez, R. H., Puls, J., McCarthy, J. K. 1997, IAUS, 180, 64

Li J., Harrington J.P. & Borkowski K.J. 2002, AJ, 123, 2676L

Liller, M. H., & Liller, W. 1968, in IAU Symp. 34, Planetary Nebulae, ed. D. E. Osterbrock & C. R. ODell (Dordrecht: Reidel), 38 (LL68)

López, J. A., Richer, M. G., García-Díaz, M. T., Clark, D. M., Meaburn, J., Riesgo, H., Steffen, W., & Lloyd, M. 2012, RevMexAA, 48, 3

Maciel, W. J. 1981 Astro. Ap. Suppl., 44, 123 Gonçalves, D. R., Villaver, E., Mampaso, A., Perinotto, M., Schwarz, H. E., & Zanin, C. 2000, ApJ, 535, 823

Guerrero, M.A., Chu, Y.-H., Gruendl, R.A., Meixner, M., 2005, A&A, 430, L69-L72

Meaburn, J., López, J. A., Gutiérrez, L., Quiróz, F., Murillo, J. M. & Valdéz, J. 2003, RMxAA, 39, 185M

Méndez, R. H., Urbaneja, M.A., Kudritzki, R. P. & Prinja, R. K. 2011, in IAU Symp 283, Planetary Nebula: An Eye to the Future, ed. A. Manchado, L. Stanghellini, & D. Schoenberner (Cambridge University Press), 436

Natta, A., Pottasch, S. R., & Preite-Martinez, A., 1980, A&A, 84, 284

O'Dell, C. R., Ferland, G. J., Henney, W. J., & Peimbert, M. 2013, AJ, 145, 170

O'Dell, C. R. & Henney, W. J., 2008, AJ, 136, 1566

O'Dell, C. R., Weiner, L. D., & Chu, Y. H. 1990, ApJ, 362, 226

Pauldrach, A. W. A., Hoffmann, T. L., & Mendez, R. H. 2004, A&A, 419, 1111

Pottasch, S. R., Surendiranath, R. & Bernard-Salas, J. 2011, A&A, 23, 531A

Pottasch, S. R., Bernard-Salas, J. & Roelling T. L. 2008, A&A, 481, 393

Ruiz, N., Chu, Y.-H., Gruendl, R.A., Guerrero, M.A., Jacob, R., Schnberner, D., Steffen, M., 2013, ApJ, 767, 35, 11pp.

Tinkler, C. M., Lamers, H. J. G. L. M. 2002, A&A, 384, 987

Ueta, Toshiya, Murakawa, Koji, Meixner, Margaret. 2006, ApJ, 641, 1113U

Stanghellini, L., Shaw, R. A., & Villaver, E. 2008, ApJ, 689, 194

Steffen, Wolfgang, & Koning, Nico. 2011, AJ, 141, 76S

Szyszka, C., Zijlstra, A. A., & Walsh, J. R. 2011, MNRAS, 416, 715S